analytical chemistry

pubs.acs.org/ac Article

A Three-Dimensional Printed Inertial Microfluidic Platform for Isolation of Minute Quantities of Vital Mitochondria

ChiaHung Lee, Yumay Chen, Ping Wang, Douglas C. Wallace, and Peter J. Burke*

Cite This: https://doi.org/10.1021/acs.analchem.1c03244 Read Online

ACCESS | Metrics & More | Article Recommendations | Supporting Information

ABSTRACT: We demonstrate a fast and easy-to-use three-dimensional printed microfluidic platform for mitochondria isolation from cell and tissue lysates based on inertial microfluidics. We present and quantify the quality of the isolated mitochondria by measuring the respiration rate under various conditions. We demonstrate that the technology produces vital mitochondria of equal quality to traditional, but more burdensome, differential centrifugation. We anticipate that the availability of improved tools for studies of bioenergetics to the broader biological community will enable these and other links to be explored in more meaningful ways, leading to further understanding of the links between energy, health, and disease.

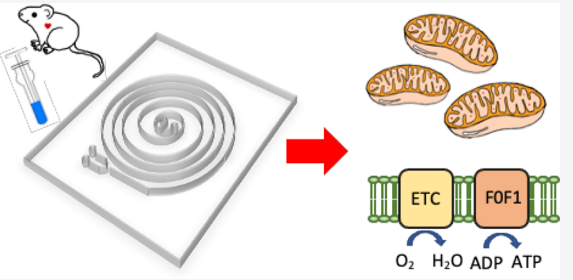

Downloaded via UNIV OF CALIFORNIA IRVINE on May 3, 2022 at 17:53:39 (UTC).
See https://pubs.acs.org/sharingguidelines for options on how to legitimately share published articles.

INTRODUCTION

Mitochondria play a critical role in life, death, and pathology.[1−6] Assays of mitochondrial function such as membrane potential, respiration rate, and pH provide a host of information about these electro physiologically active organelles.[7,8] To dissect the function, it is necessary in many cases to remove mitochondria from cells or tissues for further analysis. Although contextual information is lost, significant control is gained, similar to how single-cell analysis provides important information about cellular biology, even though cells are removed from the organism.

Mitochondria burn dietary calories using oxygen to provide the chemical energy needed to do work, maintain ATP levels, and heat to maintain body temperature. As a toxic by-product, mitochondria produce much of the endogenous cellular oxygen radicals or reactive oxygen species, a process believed to eventually result in declining organ function, aging, and death.[9] A growing body of evidence suggests that the regulation of metabolism is important in an even wider variety of biological processes, including stem cell differentiation, cancer,[10] neurodegenerative diseases, and diabetes.[5,6,11,12] As a specific example, inheritance patterns of one of the electron transport chain complexes (complex II, succinate dehydrogenase) have identified succinate dehydrogenase as a tumor suppressor gene, although the mechanism that relates to the defect in this particular electron transport chain component and tumorigenesis is still not understood in detail.[6,13−21] We anticipate that the availability of improved tools for studies of bioenergetics to the broader biological community will enable these and other links to be explored in more meaningful ways, leading to further understanding of the links between energy, health, and disease.

Exquisite, precise studies of the electron transport chain are possible in isolated mitochondria, as opposed to whole, intact cells. The electron transport chain is a set of four mitochondrial inner membrane protein complexes that use the chemical energy stored in pyruvate to pump protons out of the inner matrix and maintain an electrochemical gradient across the mitochondrial inner membrane ($\Delta P = \Delta\Psi_m + \Delta\mu^{H+}$). $\Delta\Psi_m$ is a voltage, whereas $\Delta\mu^{H+}$ is a pH gradient (typically less significant). The fifth complex (ATP synthase) uses the membrane potential to drive the phosphorylation of ADP to ATP. The rate of mitochondrial respiration and the oxygen consumption of freshly isolated mitochondria is measured in many labs[22] using various substrates and inhibitors (as well as other regulatory chemistries, such as ATP/ADP ratio, Ca^{++}, and other mimics of the cytoplasm) to differentiate the function of the five key complexes of the electron transport chain.[23,24] Although not identical to their exact behavior in intact cells,[22] these studies of each component of the electron transport chain allow exquisite, sensitive measures of mitochondrial components not possible in whole cells.

A traditional isolation process relies on mechanical lysis of the cell plasma membrane followed by a differential centrifugation.[23,25] The mitochondria are only viable for about an hour after this process (i.e., they consume oxygen,

Received: July 30, 2021
Accepted: April 18, 2022

© XXXX American Chemical Society

convert ADP to ATP, and sustain a membrane potential). There is significant risk to damage of the mitochondrial membrane integrity. Common methods for mitochondria isolation are through the density-gradient centrifugation or immune-isolation method; both require processing such as cell lysis, fractionation, and purification and usually take around 2−3 h, while the isolated mitochondria are vulnerable and can only survive a few hours after sorting processes. In addition, the disruption and damage caused during centrifugation procedures to the fragile mitochondrial membranes could also harm its functionality. These become an obstacle for mitochondria research and clinical applications. As a result, it is critical to have a fast, stable, and validated technology to isolate and assay vital mitochondria from cells and tissues.

Reproducibility of mitochondrial assays is also an issue. In a study published in 2004,[26] a set of tissue from the bovine skeletal muscle was divided and sent to 14 different labs around Europe. In this blind study, each lab was asked to assay the activity of the mitochondrial complexes using spectrophotometry. Note that this did not require intact organelles, only active enzyme complexes. Thus, this test was less stringent than the technology we aim to present here, which is to assay the respiration of an intact organelle. Nevertheless, in spite of this very straightforward assay, the labs came up with varying results that were off in the simple metric of enzyme activity by up to an order of magnitude. These are assays on which clinical decisions are made, and research is based on these assays. Therefore, we claim that there is a reproducibility issue with mitochondrial functional assays.

Microfluidic isolations using inertial microfluidics for micrometer and sub-micrometer particles have been utilized in multiple biological applications in the past decade (e.g., WBC and RBC sorting, CTC detection, and viral recovery from blood[27−35]). Among all applications, inertial microfluidics stands out as one of the most promising solutions for mitochondria isolation without damage to the membrane and function.[29] The mechanism of inertial microfluidics separating particles utilizes the balancing of inertial lift force and the "Dean" drag force to drive particles to different equilibrium positions in the microchannel based on their sizes. To manipulate single-micron size or sub-micron size particles, further investigation in channel geometry designs has been done, for example, spiral, serpentine, or trapezoidal spiral channel designs to induce secondary flow and thus enhance the Dean drag forces for small particle concentrations. However, the complexity of the channel structure brings up difficulties in traditional SU8 photolithography fabrication. Recently, additive manufacturing has become a powerful platform to fabricate three-dimensional (3D) functional microfluidic systems from polymeric materials.[33] Benefiting from the stereolithography apparatus (SLA) technique, the resolution for microfabrication and prototyping has reached under 100 μm, which has met the criteria for most microfluidic applications.

Tesauro et al.[29] demonstrated the feasibility of using inertial microfluidics to isolate mitochondria from cell lysates. They followed the SU8 soft-lithography techniques generating a four-loop spiral geometry PDMS channel and were able to reach up to 90% isolation efficiency. In their research, the apurinic/apyrimidinic endonuclease 1 (APE1) activity of unsorted and sorted liver mitochondria was measured to validate whether the retrieved mitochondria retain the biological functionality. However, to evaluate the dysfunction of isolated mitochondria, the gold standard is through measurements of mitochondrial respiration as electron transport chain and oxidative phosphorylation reflect the concerted function of intact, fully functional mitochondria. The isolation procedure can easily leave functional "pieces" of mitochondria such as active enzymes, but only respiration demonstrates the function of the entire organelle. Until now, all previous papers related to mitochondria isolation using inertial microfluidics demonstrated only proof of vitality and function of mitochondria, such as the ATP assay, ROS measurement, or MitoTracker dyes.

To quantify organelle integrity, the respiratory control ratio (RCR) is usually used.[7,8] This empirical parameter is based on the observation that mitochondria damaged during isolation show an increased proton leak of the inner membrane as compared to undamaged mitochondria, hence an increased state 4 respiration rate. The RCR is typically defined as the ratio of the state 3 to state 4 respiration rate (achieved using different substrates for the electron transport chain). The RCR assay thus measures the "leakage" of membrane potential quantitatively: Higher RCR means less damage to the mitochondria during the isolation process.

In this research, we demonstrate a fast and easy-to-use 3D printed microfluidic platform for mitochondria isolation based on inertial microfluidics. We present and quantify the RCR of this isolation technology and protocol and demonstrate that it produces vital mitochondria from cell lysates with the same quality (measured via the RCR) as mitochondria isolated using benchtop centrifuges. The advantages of this are (i) automated vs manual centrifugation step, reducing operator dependence of the process; (ii) ability to isolate small quantities of mitochondria; and (iii) the possibility to integrate with other on-chip assays such as on-chip cell lysis,[36] mitochondrial sorting, membrane potential, pH assays,[37−39] and even single mitochondria respiration assays.[40] Additional possible advantages include the following: (i) Time to analysis from cell harvest to mitochondrial downstream functional analysis is dramatically shortened (a few minutes vs an hour) as compared to centrifugation and mechanical lysis. Once isolated, the mitochondria are immediately available for subsequent downstream analysis. (ii) Oxygenation stability. The samples are not subject to repeated cycles of hypoxia/normoxia, an inadvertent side effect of multiple centrifugation steps, and a potential complication for studies of metabolism. (iii) Thermal control. The demonstrated process allows control of the temperature during the isolation and analysis process. Many of the centrifugation processes require changes in temperature, and some assays do not allow temperature control at all. (iv) Mechanical protection. In contrast to mechanical centrifugation, the demonstrated process is extremely gentle.

The intended use case for this technology is where cell materials are sparse or rare, such as in patient biopsies or research applications where large quantities of the starting tissue are prohibitively expensive. Such may be the case, for example, in personalized medicine[41,42] where specific chemotherapies where mitochondria isolated from tumor biopsies are treated in vitro with different target chemotherapies to decide on a course of treatment for a patient.[43] Another example is in muscle biopsies of babies and young children, where the absolute minimum amount of tissue is desired in this painful procedure. Another example is in the case of assaying mitochondria from a single cell. None of the above use cases

https://doi.org/10.1021/acs.analchem.1c03244
Anal. Chem. XXXX, XXX, XXX−XXX

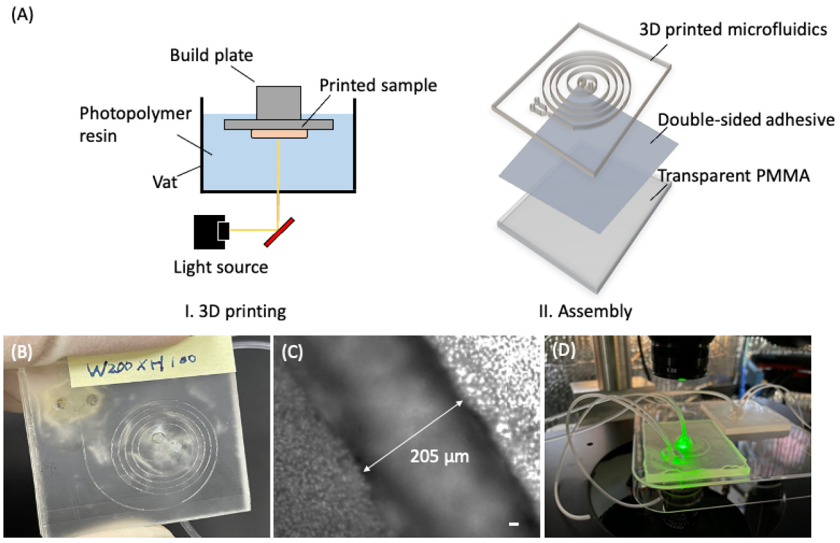

Figure 1. Fabrication and imaging setup. (A) Manufacturing process of (I) 3D printing and (II) microfluidic platform assembling. (B) Picture of the 3D printed microfluidic platform. (C) Channel dimension check under the microscope (channel width: 205 μm; 20×, scale: 20 μm). (D) Microfluidic platform on the imaging system.

is possible with traditional isolation techniques based on differential centrifugation. All the examples above are enabled by the technology presented in this paper.

SEPARATION MECHANISM

In the Navier−Stokes equation at low Reynolds numbers, the Stokes ($F = ma$) terms are usually set to zero, which is equivalent to neglecting the effect of inertia on the fluid flow. However, in microfluidic systems, this is not completely justified.[28,44] While fluid flow remains laminar (since turbulence typically sets in at around $R \sim 2000$), non-trivial inertial effects become apparent and can be exploited and engineered. The key effect in curved microfluidic channels is that these inertial effects give rise to secondary flow effects not considered in most laminar flow applications, the most dominant being the generation of two symmetric vortices in the channel called "Dean's vortices".[45] The dimensionless "Dean number (De)" captures the magnitude of this effect. The calculation of De is given by

$$De = \frac{\rho U_f D_h}{\mu}\sqrt{\frac{D_h}{2R}} = Re\sqrt{\frac{D_h}{2R}}$$

where ρ is the density of the fluid medium, U_f is the average fluid velocity, μ is the fluid viscosity, R is the radius of curvature of the channel, D_h is the hydraulic diameter of the channel, and Re is the flow Reynolds number. In our system, we estimate that Re is around 6.65 and De is around 0.9 (Supporting Information).

In spiral or curvilinear channels, the interplay of the net inertial lift force (F_L) and Dean drag force (F_D) gives rise to the Dean coupled inertial migration of particles. The ratio of inertial lift force to Dean drag force is a key parameter (R_f) to characterize particle inertial focusing. This inertial force ratio, $R_f = a^2R/D_h^3$, is useful for predicting particle behavior where R is the largest radius of curvature in the system. For particle focusing in a continuously curving channel, it is observed that the R_f needs to be >0.04[28] (or $a/D_h > 0.07$[46]). In our designed channel size, the a/D_h ratio is around 0.01 for isolated mitochondria, which indicates that the inertial lift forces will be small on particles with sizes as small as mitochondria. Therefore, instead of concentrating on the mitochondria, we are trying to concentrate the large debris and thus separate them from mitochondria. We choose the double-inlet Spiral/Dean flow fractionation (DFF[47]) to achieve the isolation of smaller micro- or nanometer-sized elements through well-controlled Dean migration. We also discuss the friction effect due to the channel roughness in the Supporting Information.

A particularly important use case is the separation of particles based on their physical properties[27,29−35] such as size, charge, mass, etc. The Dean flow-based force will exhibit different drags on different particle sizes as they sample different flow velocity field profiles. This has been exploited for two types of separation: "soft" and "hard" particles. The "hard" particles are latex beads done mostly for test and demonstration purposes. The "soft" particles are blood cells, which have a deformable lipid bilayer cell wall. Only one case of mitochondria has been shown. Mitochondria can be considered somewhere between soft and hard as the lipid bilayer is rich in cardiolipin giving different mechanical properties as compared to cell walls and because the viscosity of the internal matrix of mitochondria is much higher than the cytoplasm. These are only qualitative statements as a detailed mechanical model of the deformation properties of isolated mitochondria has never been published and is not known quantitatively. For this reason, also, one should not expect experiments in either cells or latex beads to be representative of mitochondria separation experiments.

In spite of this uncertainty, Tesauro et al.'s report[29] has shown interior microfluidic separation, but they did not show the vitality of the isolated mitochondria and they used photolithography. In our work, we have scaled the channel dimensions of their design by 2× (h = 50−100 μm, w = 100−200 μm) to relax the manufacturing tolerance due to the simplified 3D printing technology we used. This gave rise to comparable flow velocities; the channel area was 4× larger in our work, and the optimal flow rate was 3× larger (60 vs 20 μL/min). Their hydraulic diameter was 66.7 μm vs ours at 133.3 μm. Therefore, the mechanism of separation in our work vs Tesauro et al.'s is expected to be the same. In spite of a lack

https://doi.org/10.1021/acs.analchem.1c03244
Anal. Chem. XXXX, XXX, XXX−XXX

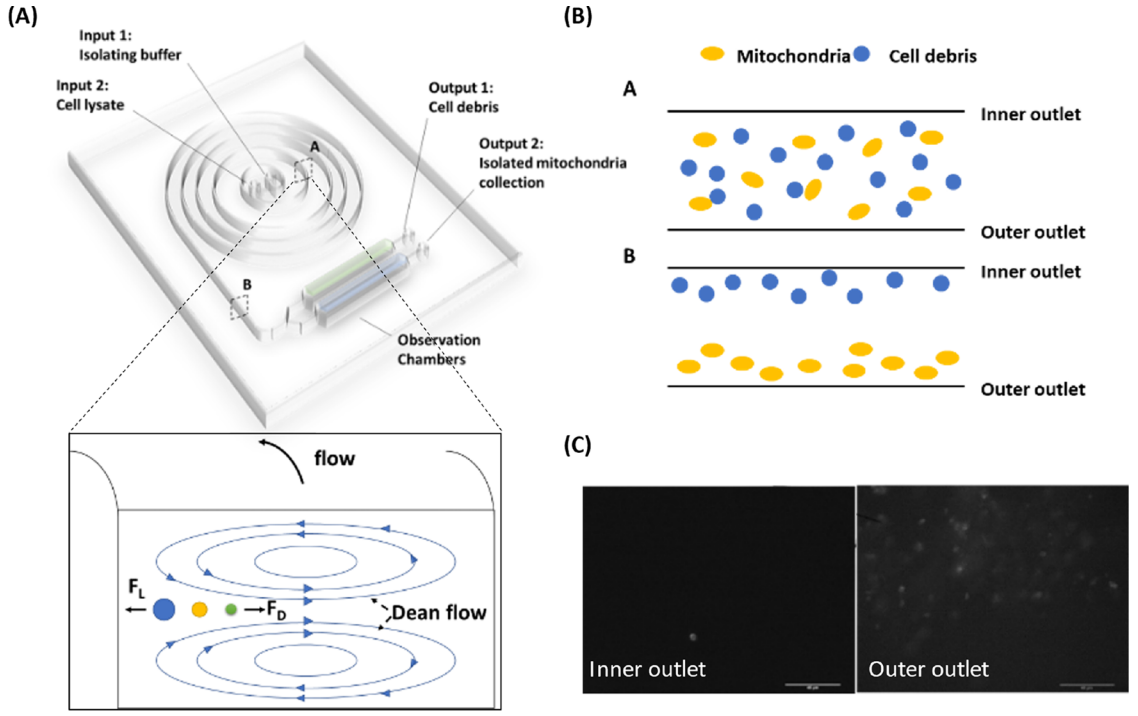

Figure 2. Schematic figure for the inertial microfluidic platform of mitochondria isolation. (A) The cross-section A and B show the migration of isolated mitochondria undergoing secondary flow and (B) the final distribution of mitochondria and cell debris. (C) Collection of isolated mitochondria stained with MitoTracker Green from the inner outlet and from the outer outlet (40× objective, scale: 20 μm).

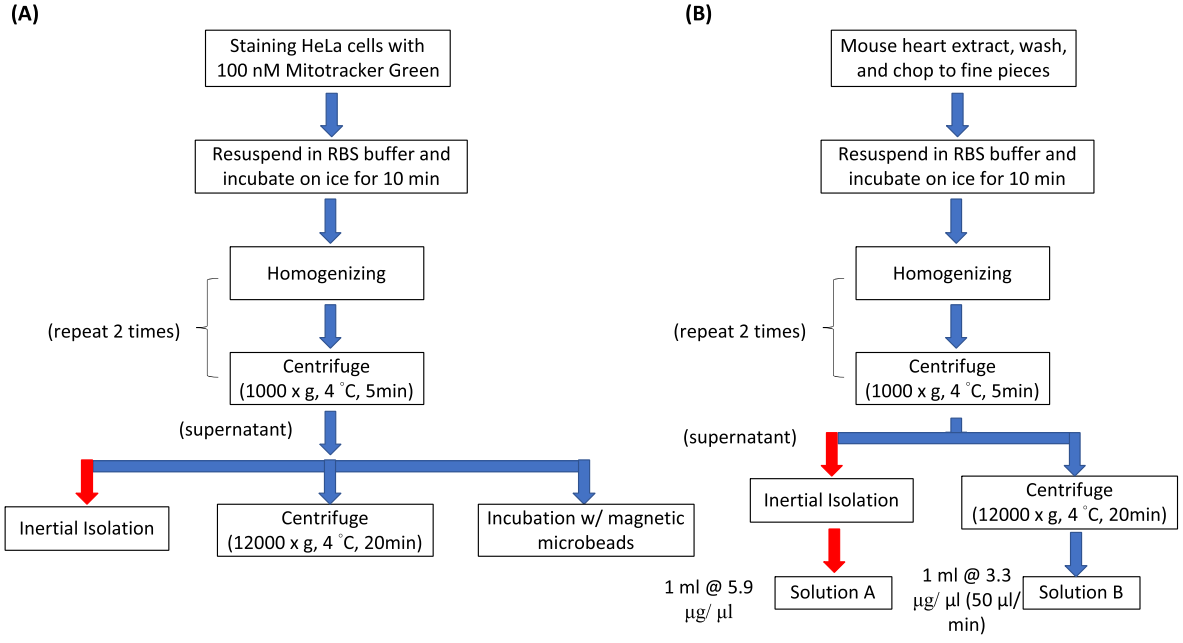

Figure 3. Protocols for isolation of mitochondria retrieved from (A) cell culture and (B) fresh mouse cardiac tissues.

of a detailed quantitative model of the separation mechanism, the method works, once optimized for flow rates, and does not damage mitochondria, in our extremely low cost to produce 3D printed channels. We now discuss in more detail the inertial lift force in our geometry. The inertial lift force is predicted to asymptotically scale as U^2/H^2 for fixed particle size and medium density,[28,48] where U is the mean flow velocity and H is the channel dimension. Therefore, the lift force for our geometry is comparable to that of the narrower channels in Tesauro et al.'s since our H is 2× larger, and our U is 3× larger. Thus, in our work, consistent with Tesauro et al.'s, the inertial lift force for mitochondrial particles is sufficient for separation and concentration.

The mechanism of separation is a balance of the inertial lift force and the Dean drag force. In contrast to prior work where separation of particles of different sizes is achieved, we only seek to separate mitochondrial particles from everything else, similar to the way a high g centrifuge separates mitochondrial particles but does not sort particles based on size. The detailed balance of forces can in principle be simulated and calculated,

https://doi.org/10.1021/acs.analchem.1c03244
Anal. Chem. XXXX, XXX, XXX−XXX

but this is notoriously difficult to perform precisely. For example, in Di Carlo's report[28] and Zhang et al.'s report,[44] it is stated that "the exact mechanism and location of the superposition of secondary flow and lift effects are complex and unknown experimentally and theoretically such that I currently can only speculate in Figure 5 on the precise combined behavior." Thus, similar to the literature, we are only demonstrating that the two forces can be balanced but not providing a detailed location within the channel that they are focused on the equilibrium concentration. In contrast to other literature, we are not separating different particles of the minor difference in size but only separating mitochondrial particles from much larger cellular debris such as the nucleus as well as much smaller molecular contents, such as RNA and ribosomes.

EXPERIMENTAL METHODS

Platform Design and Fabrication. In this study, an inertial microfluidic platform was fabricated using a high-resolution SLA 3D printer (Peopoly Moai) featuring 70 μm XY resolution and 25 μm Z resolution (Figures 1 and 2). The platform was first drafted using commercial CAD drawing software (Solidwork) and transformed into STL format. The file was then sliced in the Z direction using Ultimaker Cura software. The sliced file was then sent to the 3D printer with a UV wavelength of 405 nm. The UV light was projected from the bottom of the resin bath. Afterward, the platform was cleaned with ethanol and exposed to a UV light with 405 nm wavelength within a curing chamber for the post curing process. The channel width was 200 μm with 500 μm spacing in between, and the channel height was 100 μm. The design was based on the principle described in Bhagat et al.'s report[49] with a/D_h ratio of ~0.01, where a is the diameter of the particle and D_h is the hydraulic diameter of the channel. Later, tubes were connected to the microchannel by tweezers and sealed with epoxy instant mix glue (Loctite) to form the closed microchannels. ARcare 90445, a medical grade pressure-sensitive double-sided adhesive (Adhesive Research), was attached onto the platform to seal and form the closed channel, while the other side was attached to a rigid and transparent plastic plate to avoid tape debonding caused by high injecting pressure during fluidic manipulation.

Preparation of Mitochondria from the HeLa Cell Culture. HeLa cells used in this research were purchased from ATCC. The cells were cultured for 2−3 days in 75 cm^2 tissue flasks at 37 °C and 5% CO_2. MitoTracker Green (ex/em 490/516 nm) at 100 nM was added and incubated for 30 min. The protease trypsin was used to detach cells from the flask, and the same amount of medium was later added to stop the reaction. The cell collections were centrifuged for 5 min at 1000g, and the pellets were resuspended in ice-cold RBS buffer (5 mM KCl, 1 mM $MgCl_2$, 20 mM HEPES (pH 7.0)) and incubated on ice for 10 min. After incubation, the solution was transferred into a glass homogenizer and we performed 40 strong strokes separately using loose and tight stroking. The homogenate was then recentrifuged at 12,000g for 20 min at 4 °C. The collected supernatant was the isolated mitochondria. Figure 3A shows the common procedures of mitochondria isolation through differential centrifugation, immune capturing with magnetic microbeads, and inertial microfluidics. Fluorescence imaging of isolated mitochondria from cultured cells was used to observe the migration results under inertial focusing.

Preparation of Mitochondria from the Mouse Heart. A fresh mouse cardiac tissue was retrieved using established methods.[50] After retrieval, the minced tissue was transferred into a falcon tube with 5 mL of ice-cold RBS buffer (5 mM KCl, 1 mM $MgCl_2$, 20 mM HEPES (pH 7.0)) added and the tube was then incubated on ice for 10 min. After incubation, the solution was transferred into a glass homogenizer and we performed 40 strong strokes separately using loose and tight stroking. Next, we centrifuged the homogenate at 1000g for 5 min at 4 °C to remove large-scale debris. Half of the supernatant was collected for inertial microfluidic testing use (Solution B), and the rest was recentrifuged at 12,000g for 20 min at 4 °C as a control sample of purified isolated mitochondria using standard methods. The pellet was collected and resuspended in RBS buffer (Solution A) as the comparison group (Figure 3B). All animal experiments were carried out in an ethical manner, in accordance with the protocols approved by the IACUC committees at the University of California, Irvine.

Microscopy and Image Analysis. Slides were analyzed with an Olympus IX71 microscope using 20× (LUCPlanFLN, 20×, NA = 0.45, Olympus) and 40× objectives (PlanApo 40×, NA = 0.95, Olympus). The fluorophores were excited by UV LEDs (M490L3, 350 mA, THORLABs). Fluorescence signals from MitoTracker Green were selectively filtered through a dichroic and bandpass filter (excitation: 490 nm, emission: 516 nm).

Mitochondria Respiration Assay. An Agilent Seahorse XFe24 analyzer was used for measuring the oxygen consumption rate (OCR) of isolated mitochondria according to established protocols.[51] This provides a standard and comprehensive method of assessing the key parameters of mitochondrial function in isolated mitochondria: basal respiration, ATP-linked respiration, H+ (proton) leak, maximal respiration, spare respiratory capacity, and non-mitochondrial respiration. The respiratory control ratio (RCR) can easily be calculated as the ratio of state 3 to state 4 respiration.

After the protein concentration is determined, aliquots of the isolated mitochondria solution were inserted into the wells (10 μg/well, at least 4 wells/sample) at a final concentration of 10 μg of mitochondria in 50 μL of 1× MAS buffer (Sucrose 70 mM, Mannitol 220 mM, KH_2PO_4 10 mM, $MgCl_2$ 5 mM, EGTA 1 mM, fatty acid free BSA 0.2%, PIPES 25 mM, pH 6.8 at 37 °C) with substrates (5 mM pyruvate and 5 mM malate). Mitochondria were plated onto a Seahorse culture plate and centrifuged at 2000g for 20 min at 4 °C. MAS (450 μL, 1×) was added to each well and incubated at a 37 °C, non-CO_2 incubator for 8 min.

The four injection ports were filled with (i) 55 μL, 40 mM ADP, (ii) 60 μL, 25 μg/mL oligomycin, (iii) 65 μL, 40 μM FCCP, and (iv) 70 μL, 40 μM Rotenone. The experimental procedure is described below:

1. Measuring the basal respiration of isolated mitochondria.
2. Adding ADP, rapid oxygen consumption, and the formation of ATP (state 3).
3. Adding oligomycin, the ATP synthesis inhibitor (state 4).
4. Adding FCCP, the uncoupler.
5. Adding Rotenone, interfering with complex I in the ETC.

Definition of Isolation Efficiency. To determine the isolation efficiency of the inertial microfluidic method, 1 mL of

https://doi.org/10.1021/acs.analchem.1c03244
Anal. Chem. XXXX, XXX, XXX−XXX

the retrieved mitochondria concentrations from both inner and outer outlets was measured using the Bradford assay. For example, the isolated mitochondria concentrations under a flow rate of 50 μL/min were measured to be 1.58 μg/μL in the inner outlet and 3.33 μg/μL in the outer outlet. The isolation efficiency was then defined as 3.33/(1.58 + 3.33) = 68%. To determine the isolation efficiencies versus the flow rates, three distinct measurements were examined under each flow rate.

RESULTS

The retrieved amount of the isolated mitochondria concentration using the inertial microfluidic method relies on (i) the concentration of lysate and (ii) the length of isolating time. Unlike the centrifugation method having a fixed isolation time, the inertial method is more suitable for a small amount of requirements (10 pg of mitochondria can be sorted out in 5 s with the inertial microfluidic method compared to 20 min in the traditional centrifugation method).

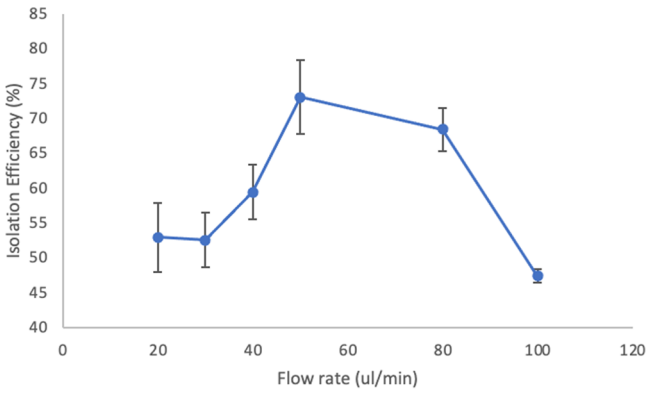

Figure 4. Isolation efficiency of mitochondria under different flow rates using inertial microfluidics.

Isolation Efficiency vs Flow Rate. Although there has been extensive theoretical and computation analysis of ideal submicron particles such as latex beads,[27−35] the exact parameters for mitochondria isolation need to be determined empirically due to the lack of models with enough sophistication to predict quantitative yield. Thus, the optimized flow rate for sorting was determined empirically. From our experiences, an average of up to 73% of mitochondria could be retrieved from the inner outlet when using a flow rate of 50 μL/min (Figure 4).

Oxygen Consumption Rate for Isolated Mitochondria. To further investigate whether the retrieved mitochondria retain their biological functionality, an Agilent Seahorse XFe24 analyzer was used for measuring the oxygen consumption rate (OCR) of isolated mitochondria. The isolated mitochondria under 50 μL/min flow rate were tested and compared to the traditional centrifugation method. A measure of "coupling" that retains utility is the respiratory control ratio (RCR), an empirical parameter frequently used for assessing the integrity of the mitochondria preparation (Figure 5).

The respiratory control ratio (RCR) was from state 3 (ADP)/state 4 (oligomycin). The RCR value from the mitochondria from the control group is used as the indicator of the quality of the mitochondrial preparation. As the result showed, the RCR values are calculated to 3.9 $\pm$ 0.7 and 3.8 $\pm$ 1.5 corresponding to isolated mitochondria that undergo the centrifugation method and inertial microfluidic method with 50 μL/min, respectively. The error bars are according to the measurements of multiple wells. This work has shown for the first time the use of microfluidic centrifugation for isolation of vital mitochondria. The RCR is as good as or better than traditional differential centrifugation.

The fact that the results from inertial microfluidic and traditional centrifugation give rise to no difference in the respiration results in Figure 5 is the most important point of this work: This proves that the inertial microfluidic method, with all of its advantages (discussed in more detail below), produces isolated mitochondria with the same quality and quantitative properties of mitochondria isolated and studied with traditional centrifuges, a body of knowledge that has been proven over 30 years of research and thousands of papers.[7]

DISCUSSION

The motivation of this work is to build a fast and solid method for a small amount of requirements of isolated mitochondria. In Table 1, we compare and summarize our proposed inertial

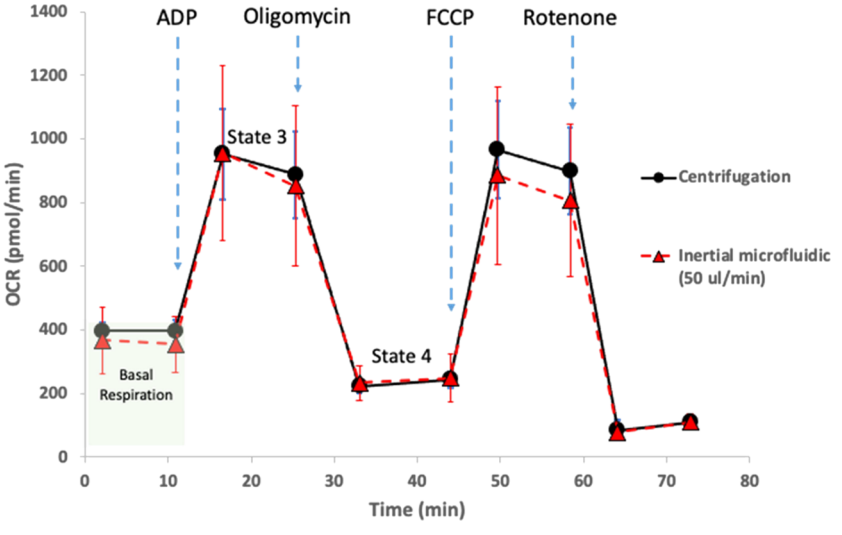

Figure 5. Oxygen consumption rate (OCR) of isolated mitochondria under different isolation procedures and conditions.

https://doi.org/10.1021/acs.analchem.1c03244
Anal. Chem. XXXX, XXX, XXX−XXX

Table 1. Comparison of Mitochondria Isolation between the Centrifugation Method and Inertial Microfluidic Method Proposed in This Article

mechanism	yield	duration	pros	cons
1. differential centrifugation (DC)	7−50 μg per 10^6 cells (depends on cell types)	90−120 min	Cultured cells are standardized models and easily obtained.	The integrity of mitochondria must be checked carefully after isolation.
			Mitochondria of higher purity can be prepared using a sucrose gradient.	All the experiments that require intact mitochondria must be performed within 3 h after isolation.
2. antibody- coated magnetic beads[52]	~4 times more than the ultracentrifugation method	15−60 min of incubating mitochondria with antibody-coated magnetic beads	This has high purity of isolated mitochondria.	Mitochondria cannot be released from magnetic beads. This may affect the mitochondrial ultrastructure and/or cover epitopes on the mitochondrial outer membrane.
3. affinity purification using magnetic beads[53]	100 μg of mitochondria from 1 g of wet yeast		This has high purity of isolated mitochondria.	This is not suited for large amounts of mitochondrial preparation.
			Mitochondria are released from magnetic beads.	Centrifugation is required.
			This does not require a large number of starting materials and ultracentrifugation.	Incubation time highly affects the isolation efficiency.
4. MITO-Tag[54]	N/A	3.5 min immunoprecipitation with anti-HA bead	Epitope-tagged recombinant protein increases sensitivity.	Transfection of epitope-tagged constructs is required.
			This has the utility for assessing mitochondrial metabolism in vivo.	
5. inertial microfluidics(this proposal)	2 pg per second	depends on the number of mitochondria needed (seconds−minutes)	This simply injects lysate through a microfluidic channel.	This requires a small number of mitochondria.
				This is a continuous batch process.
				The equipment is simple and does not need training.

microfluidic method to the differential centrifugation (DC), antibody-coated magnetic beads, affinity purification using magnetic beads, and MITO-Tag.

DC is the most common laboratory method with standardized procedures and is suitable for most kinds of cell lines. DC is also suitable for preparing a massive number of mitochondria. The disadvantage of DC is that the entire protocol takes about 1−2 h, and the centrifugation procedure could cause disruption to mitochondria. Therefore, the integrity of mitochondria must be checked carefully after isolation. Magnetic beads coated with antibodies have been used to isolate mitochondria in many reports. Horing-Do et al.[52] propose using microbeads conjugated to anti-TOM22 antibodies to achieve mitochondria isolation in a high gradient magnetic field. The purity of mitochondria isolated in their protocol is comparable to mitochondria obtained using the ultracentrifuge method. However, this separation procedure takes approximately an hour from initial cell homogenization and the mitochondria cannot be released from magnetic beads, which may affect the mitochondrial ultrastructure and cover epitopes on the mitochondrial outer membrane. To minimize the interference in subsequent mitochondria structural or functional studies, Liao et al.[53] apply the concept using nickel ions to isolate recombinant proteins that are tagged with multiple histidine (His) residues to isolate highly purified mitochondria from yeast. The mitochondria concentrated from cells expressing Tom70−6xHis were incubated with Ni-NTA magnetic beads and then separated under magnetic fields. However, ultracentrifuge is required in their protocol and the incubation time of mitochondria with magnetic beads highly affects the isolation efficiency. Another example is from Bayraktar et al.[54] presenting MITO-Tag mice, which enable rapid isolation of mitochondria from specific cell types in vivo (3−5 min). Instead of using an endogenous outer membrane protein, they chose an epitope-tagged recombinant protein[55] to be the immunopurification handle because of the high sensitivity and specificity of various epitope tags and their cognate antibodies. By controlling the expression of Cre recombinase, they can restrict epitope tagging of mitochondria to a specific cell type and consequently immunoisolate mitochondria with cell-type specificity from a piece of tissue without the need for cell sorting.

On the other hand, the retrieved amount of the isolated mitochondria concentration using the inertial microfluidic method relies on (i) the concentration of lysate and (ii) the length of isolating time. Unlike the centrifugation method having a fixed isolation time, the inertial method is more suitable for a small amount of samples. For example, with this technique, 10 pg of mitochondria can be sorted out in 5 s with the inertial microfluidic method. This is approximately the number of mitochondria expected from a single cell. In Figure 5, the OCR data shows that the inertial microfluidic method can generate isolated mitochondria with integrity as good as the traditional method but faster when a small number of isolated mitochondria are required. In addition, we can always do batch processes to increase the yield and do not need a professional specialist to handle the process.

CONCLUSIONS

This work has shown for the first time the use of microfluidic centrifugation for the isolation of vital mitochondria. The RCR, the "industry standard" for the determination of the integrity and quality of the isolated organelle, is as good as or

https://doi.org/10.1021/acs.analchem.1c03244
Anal. Chem. XXXX, XXX, XXX−XXX

better than traditional differential centrifugation. We anticipate that the availability of improved tools for studies of bioenergetics to the broader biological community will enable bioenergetics to be explored in more meaningful ways, leading to further understanding of the links between energy, health, and disease, for both research and clinical diagnosis of mitochondrial diseases. Now that we can isolate mitochondria from a small number of cells, it is within the realm of possibility to push this to the single-cell level with on-chip, single-cell lysing technology. Coupled with on-chip downstream sorting and analysis of the hundreds of mitochondria from a single cell, this could enable for the first time technology to assay functional heteroplasmy of mitochondria at the single-cell level.

■ ASSOCIATED CONTENT

Supporting Information

The Supporting Information is available free of charge at https://pubs.acs.org/doi/10.1021/acs.analchem.1c03244.

SEM images for wall roughness check of the microchannel and the calculation of the Reynolds number and Dean number using the platform (PDF)

■ AUTHOR INFORMATION

Corresponding Author

Peter J. Burke − *Department of Biomedical Engineering and Department of Electrical and Engineering and Computer Science, University of California, Irvine, California 92697, United States;* orcid.org/0000-0002-8883-1014; Email: pburke@uci.edu

Authors

ChiaHung Lee − *Department of Biomedical Engineering, University of California, Irvine, California 92697, United States*

Yumay Chen − *Department of Biological Chemistry, University of California, Irvine, California 92697, United States*

Ping Wang − *Department of Diabetes, Endocrinology, and Metabolism, City of Hope National Medical Center, Duarte, California 91010, United States*

Douglas C. Wallace − *Center for Mitochondrial and Epigenomic Medicine, Children's Hospital of Philadelphia and Department of Pediatrics, Division of Human Genetics, University of Pennsylvania, Philadelphia, Pennsylvania 19104, United States*

Complete contact information is available at: https://pubs.acs.org/10.1021/acs.analchem.1c03244

Notes

The authors declare the following competing financial interest(s): Some of the authors are in the process of commercializing IP related to mitochondrial functional assays.

■ ACKNOWLEDGMENTS

We acknowledge support from the Army Research Office through the ARO (contract nos. W911NF-18-1-0076, W911NF2010103, and W911NF1910369).

■ REFERENCES

(1) Liao, P.; Bergamini, C.; Fato, R.; Pon, L. A.; Pallotti, F. *Methods Cell Biol.* **2020**, *155*, 3−31.

(2) Wallace, D. C.; Fan, W.; Procaccio, V. *Annu. Rev. Pathol.: Mech. Dis.* **2010**, *5*, 297−348.

(3) Wallace, D. C. *Review Article Mitochondrial DNA Mutations in Disease and Aging.* **2014**, *450*, 440−450.

(4) Wallace, D. C. *Science* **1999**, *283*, 1482−1488.

(5) Wallace, D. C. *Cold Spring Harbor Symp. Quant. Biol.* **2011**, *76*, 1−16.

(6) Wallace, D. C. *Nat. Rev. Cancer* **2012**, *12*, 685−698.

(7) Nicholls, D. G.; Ferguson, S. J.*Bioenergetics*; 4th ed.; Academic Press: San Diego, 2013.

(8) Gnaiger, E.*Mitochondrial Pathways and Respiratory Control. An Introduction to OXPHOS Analysis*, 3rd ed.; Mitochondr Physiol Network 17.18. OROBOROS MiPNet Publications, 2012.

(9) Wallace, D. *Annu. Rev. Genet.* **2005**, *39*, 359−407.

(10) Hanahan, D.; Weinberg, R. *Cell* **2011**, *144*, 646−674.

(11) Wallace, D. C. *Proc. Natl. Acad. Sci. U. S. A.* **2010**, *107*, 8947−8953.

(12) Wallace, D. C.; Lott, M. T.; Procaccio, V.Mitochondrial Genes in Degenerative Diseases, Cancer and Aging. In *Emery and Rimoin's Principles and Practice of Medical Genetics*; Rimoin, D. L., Connor, J. M., Pyeritz, R. E., Korf, B. R., Eds.; Churchill Livingstone Elsevier: Philadelphia, PA, 2007; Vol. Volume *1*, pp. 194−298.

(13) King, A.; Selak, M. A.; Gottlieb, E. *Oncogene* **2006**, *25*, 4675−4682.

(14) Pasini, B.; McWhinney, S. R.; Bei, T.; Matyakhina, L.; Stergiopoulos, S.; Muchow, M.; Boikos, S. A.; Ferrando, B.; Pacak, K.; Assie, G.; Baudin, E.; Chompret, A.; Ellison, J. W.; Briere, J.-J.; Rustin, P.; Gimenez-Roqueplo, A.-P.; Eng, C.; Carney, J. A.; Stratakis, C. A. *Eur. J. Hum. Genet.* **2008**, *16*, 79−88.

(15) Bayley, J.-P.; Devilee, P. *Curr. Opin. Genet. Dev.* **2010**, *20*, 324−329.

(16) Bardella, C.; Pollard, P. J.; Tomlinson, I. *Biochim. Biophys. Acta* **2011**, *1807*, 1432−1443.

(17) Vanharanta, S.; Buchta, M.; McWhinney, S. R.; Virta, S. K.; Peçzkowska, M.; Morrison, C. D.; Lehtonen, R.; Januszewicz, A.; Järvinen, H.; Juhola, M.; Mecklin, J.-P.; Pukkala, E.; Herva, R.; Kiuru, M.; Nupponen, N. N.; Aaltonen, L. A.; Neumann, H. P. H.; Eng, C. *Am. J. Hum. Genet.* **2004**, *74*, 153−159.

(18) Gottlieb, E.; Tomlinson, I. P. M. *Nat. Rev. Cancer* **2005**, *5*, 857−866.

(19) Frezza, C.; Pollard, P. J.; Gottlieb, E. *J. Mol. Med.* **2011**, *89*, 213−220.

(20) Frezza, C.; Gottlieb, E. *Semin. Cancer Biol.* **2009**, *19*, 4−11.

(21) Semenza, G. *J. Mol. Med.* **2011**, *89*, 203−204.

(22) Brand, M. D.; Nicholls, D. G. *Biochem. J.* **2011**, *435*, 297−312.

(23) Trounce, I. A.; Kim, Y. L.; Jun, A. S.; Wallace, D. C. *Methods Enzymol.* **1996**, *264*, 484−509.

(24) Trounce, I.; Neill, S.; Wallace, D. C. *Proc. Natl. Acad. Sci. U. S. A.* **1994**, *91*, 8334−8338.

(25) Frezza, C.; Cipolat, S.; Scorrano, L. *Nat. Protoc.* **2007**, *2*, 287−295.

(26) Gellerich, F. N.; Mayr, J. A.; Reuter, S.; Sperl, W.; Zierz, S. *Mitochondrion* **2004**, *4*, 427−439.

(27) DiCarlo, D.; Irimia, D.; Tompkins, R. G.; Toner, M. *Proc. Natl. Acad. Sci.* **2007**, *104*, 18892−18897.

(28) DiCarlo, D. *Lab Chip* **2009**, *9*, 3038−3046.

(29) Tesauro, C.; Ferrando, B.; Ma, X.; Jepsen, M. L.; Ivarsen, A. K. R.; Frøhlich, R.; Stevnsner, T.; Knudsen, B. R.; Ho, Y. P. *RSC Adv.* **2017**, *7*, 23735−23741.

(30) Choi, K.; Ryu, H.; Siddle, K. J.; Piantadosi, A.; Freimark, L.; Park, D. J.; Sabeti, P.; Han, J. *Anal. Chem.* **2018**, *90*, 4657−4662.

(31) Abdulla, A.; Liu, W.; Gholamipour-Shirazi, A.; Sun, J.; Ding, X. *Anal. Chem.* **2018**, *90*, 4397−4405.

(32) Zhu, S.; Wu, D.; Han, Y.; Wang, C.; Xiang, N.; Ni, Z. *Lab Chip* **2020**, *20*, 244−252.

(33) Razavi Bazaz, S.; Rouhi, O.; Raoufi, M. A.; Ejeian, F.; Asadnia, M.; Jin, D.; Ebrahimi Warkiani, M. *Sci. Rep.* **2020**, *10*, 1−14.

(34) Zhang, T.; Hong, Z. Y.; Tang, S. Y.; Li, W.; Inglis, D. W.; Hosokawa, Y.; Yalikun, Y.; Li, M. *Lab Chip* **2020**, *20*, 35−53.

(35) Kalyan, S.; Torabi, C.; Khoo, H.; Sung, H. W.; Choi, S. E.; Wang, W.; Treutler, B.; Kim, D.; Hur, S. C. *Micromachines* **2021**, *12*, 1−43.
(36) Marc, P. J.; Sims, C. E.; Bachman, M.; Li, G. P.; Allbritton, N. L. *Lab Chip* **2008**, *8*, 710−716.
(37) Zand, K.; Pham, T.; Davila, A.; Wallace, D. C.; Burke, P. J. *Anal. Chem.* **2013**, *85*, 6018−6025.
(38) Zand, K.; Pham, T. D. A.; Li, J.; Zhou, W.; Wallace, D. C.; Burke, P. J. *Mitochondrion* **2017**, *37*, 8−16.
(39) Pham, T. D.; Pham, P. Q.; Li, J.; Letai, A. G.; Wallace, D. C.; Burke, P. J. *Sci. Rep.* **2016**, *6*, 35907.
(40) Pham, T.; Wallace, D.; Burke, P. *Sensors* **2016**, *16*, 1065.
(41) Friedman, A. A.; Letai, A.; Fisher, D. E.; Flaherty, K. T. *Nat. Rev. Cancer* **2015**, *15*, 747−756.
(42) Letai, A.; Bhola, P.; Welm, A. L. *Cancer Cell* **2022**, *40*, 26−35.
(43) Letai, A. *Cancer Discovery* **2022**, *12*, 290−292.
(44) Zhang, J.; Yan, S.; Yuan, D.; Alici, G.; Nguyen, N. T.; Ebrahimi Warkiani, M.; Li, W. *Lab Chip* **2016**, *16*, 10−34.
(45) Berger, S. A.; Talbot, L. Y. *Annu. Rev. Fluid Mech.* **1983**, 461−512.
(46) Kuntaegowdanahalli, S. S.; Bhagat, A. A. S.; Kumar, G.; Papautsky, I. *Lab Chip* **2009**, *9*, 2973−2980.
(47) Liu, N.; Petchakup, C.; Tay, H. M.; Li, K. H. H.; Hou, H. W. *Appl. Microfluid. Syst. Biol. Med.* **2019**, 99−150.
(48) Xu, X.; Huang, X.; Sun, J.; Wang, R.; Yao, J.; Han, W.; Wei, M.; Chen, J.; Guo, J.; Sun, L.; Yin, M. *Analyst* **2021**, *146*, 7070−7086.
(49) Bhagat, A. A. S.; Kuntaegowdanahalli, S. S.; Papautsky, I. *Lab Chip* **2008**, 1906.
(50) Yang, J.-Y.; Deng, W.; Chen, Y.; Fan, W.; Baldwin, K. M.; Jope, R. S.; Wallace, D. C.; Wang, P. H. *J. Mol. Cell. Cardiol.* **2013**, *59*, 167−175.
(51) Sakamuri, S. S. V. P.; Sperling, J. A.; Sure, V. N.; Dholakia, M. H.; Peterson, N. R.; Rutkai, I.; Mahalingam, P. S.; Satou, R.; Katakam, P. V. G. *GeroScience* **2018**, *40*, 347−356.
(52) Hornig-Do, H.-T.; Günther, G.; Bust, M.; Lehnartz, P.; Bosio, A.; Wiesner, R. J. *Anal. Biochem.* **2009**, *389*, 1−5.
(53) Liao, P.; Boldogh, I. R.; Siegmund, S. E.; Freyberg, Z.; Pon, L. A. *PLoS One* **2018**, *13*, No. e0196632.
(54) Bayraktar, E. C.; Baudrier, L.; Özerdem, C.; Lewis, C. A.; Chan, S. H.; Kunchok, T.; Abu-Remaileh, M.; Cangelosi, A. L.; Sabatini, D. M.; Birsoy, K.; Chen, W. W. *Proc. Natl. Acad. Sci. U. S. A.* **2019**, *116*, 303−312.
(55) Chen, W. W.; Freinkman, E.; Wang, T.; Birsoy, K.; Sabatini, D. M. *Cell* **2016**, *166*, 1324−1337.e11.

https://doi.org/10.1021/acs.analchem.1c03244
Anal. Chem. XXXX, XXX, XXX−XXX

SUPPLEMENTARY INFORMATION

A 3D Printed Inertial Microfluidic Platform for Isolation of Minute Quantities of Vital Mitochondria

ChiaHung Lee[a], Yumay Chen[b], Ping Wang[c], Douglas C. Wallace[d], Peter J. Burke[a,e*]

[a]Department of Biomedical Engineering, University of California, Irvine, CA 92697, USA.

[b]Department of Biological Chemistry, University of California, Irvine, CA 92697, USA.

[c]Department of Diabetes, Endocrinology, and Metabolism. City of Hope National Medical Center, Duarte, CA 91010.

[d]Center for Mitochondrial and Epigenomic Medicine, Children's Hospital of Philadelphia and Department of Pediatrics, Division of Human Genetics, University of Pennsylvania, Philadelphia, PA 19104, USA.

[e]Department of Electrical and Engineering and Computer Science, University of California, Irvine, CA 92697, USA.

This Supplementary Information file includes the SEM images to show the wall roughness of the microchannel and the calculation of Reynolds number and Dean number of using the platform.

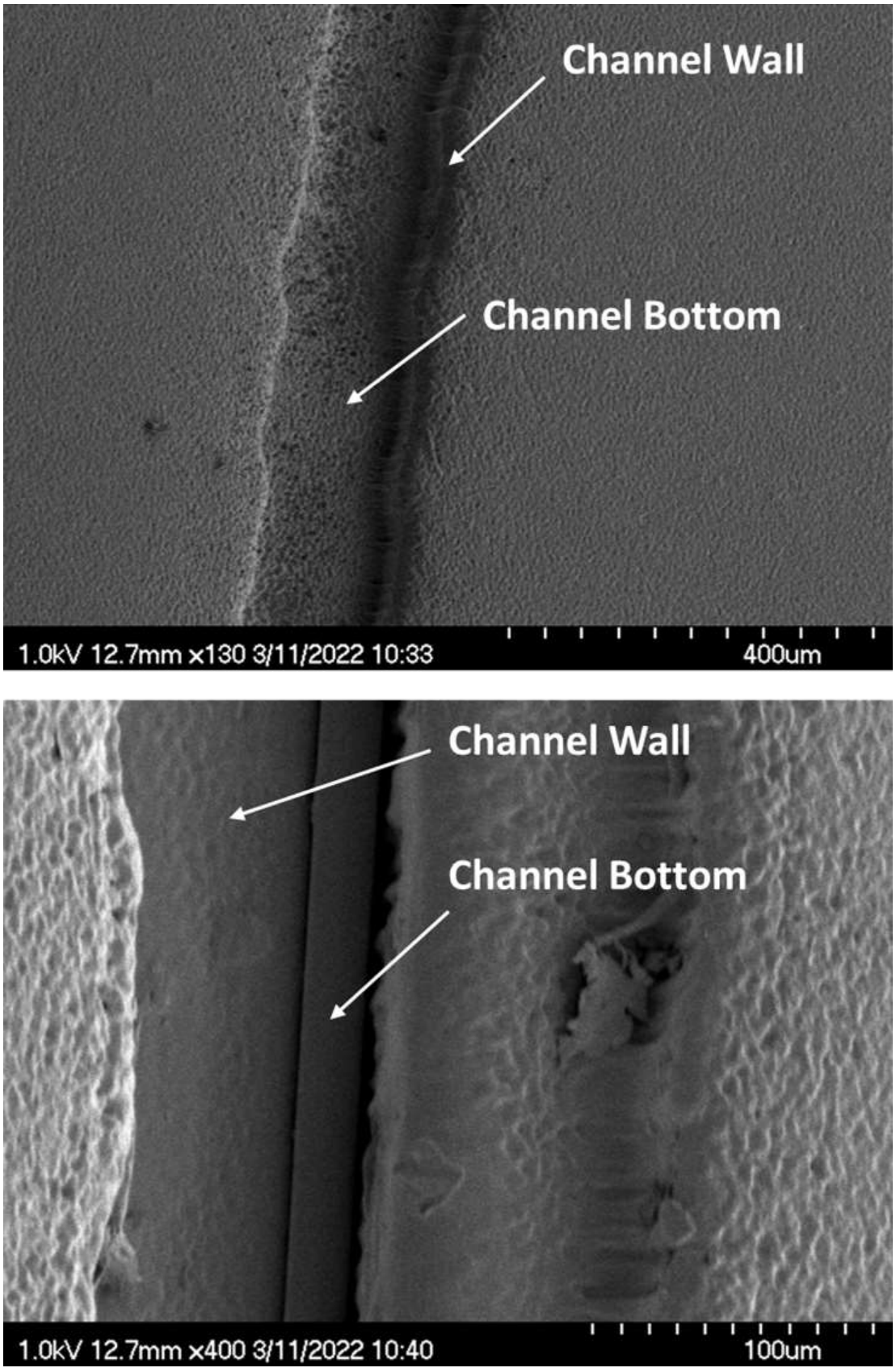

Figure S1: SEM image of microchannel sidewalls coated with 5 nm Iridium. (a) curvature channel, (b) straight channel.

Supplementary Discussion 1: Calculation of Reynolds number and Dean number

The Reynolds number (Re) is defined as the ratio of inertial force to viscous (or friction) force, and can be expressed as:

$Re = \rho u D_h / \mu$, Where

Re = Reynolds Number (non-dimensional),

ρ = density (kg/m^3),

u = velocity based on the actual cross-sectional area of the duct or pipe (m/s),

μ = dynamic viscosity (Ns/m^2),

D_h = hydraulic diameter (m), which is 4A/P, where A is the cross-sectional area of the flow, and the P is the perimeter of the cross-section.

We use the water density 1000 kg/m^3 and the dynamic viscosity is 0.001 Ns/m^2 to do the calculation.

The flowrate (Q) is calculated by A*V', where A is the cross-section area and V' is the average velocity. Therefore, the average velocity is calculated as:

60 ($\mu l/min$) / 20000 (μm^2) = $5*10^{10}$ ($\mu m^3/min$)/ ($2*10^4$) (μm^2) = $2.5 *10^6$ $\mu m/min$ = 0.05 m/s.

The hydraulic diameter is calculated by:

4*(width*height)/(2*width+2*height) = 4*(100 um*200 um)/ 600 um ~= 133 um.

Therefore, the Re is calculated as:

1000 (kg/m^3) * 0.05 (m/s) * $1.33*10^{-4}$ (m) / 0.001 (Ns/m^2) ~= 6.65.

The Dean number (De) is calculated as:

$Re*(D_h/2R)$

Where R is the radius of curvature and we calculated to be ~ 3 mm. Therefore, the De is calculated as = 6.65 * $(133(\mu m)/(2*3000)(\mu m))^{0.5}$ ~= 0.9 (order of 0.1).

Supplementary Discussion 2: Channel roughness

To determine the surface roughness of the walls, we took SEM images of the fabricated devices (Figure S1) and measure the roughness on the bottom of channel using Dektak. Based on these images we estimate the wall surface roughness to be under 2 microns. Since this is much less than the channel width, we believe this does not significantly affect the separation efficiency.